Evaluating the spatial patterns of NOx emissions in polluted areas with TROPOMI NO₂

Daniel L. Goldberg[*,1], Madankui Tao[2], Gaige Kerr[1], Siqi Ma[3], Daniel Tong[3], Arlene M. Fiore[4], Angela Dickens[5], Zac Adelman[5], Susan Anenberg[1]

[1]Department of Environmental and Occupational Health, Milken Institute of Public Health, George Washington University, Washington, DC, USA
[2]Department of Earth and Environmental Sciences, Columbia University, New York City, NY, USA
[3]Department of Atmospheric, Oceanic & Earth Sciences, George Mason University, Fairfax, VA, USA
[4]Department of Earth, Atmospheric, and Planetary Sciences, Massachusetts Institute of Technology, Cambridge, MA, USA
[5]Lake Michigan Air Directors Consortium, Hillside, IL, USA

*Correspondence to: Daniel L. Goldberg (dgoldberg@gwu.edu)

Abstract

Satellite datasets are increasingly used to evaluate NOx emissions inventories. Such studies often require the use of a chemical transport model or a complex statistical framework to account for meteorological factors that can complicate the comparison. Here, we apply a novel method to compare inventory-based emissions directly to Tropospheric Monitoring Instrument (TROPOMI) NO₂ data without a chemical transport model by accounting for the two most important meteorological factors: wind speed and direction. We oversample the satellite data over multiple years and filter to use data on stagnant wind days only, and then use this satellite average to evaluate the spatial representativeness of the 1×1 km^2 inventory-based Neighborhood Emission Mapping Operation (NEMO). In nine out of ten US cities, spatial r^2-values between NEMO NO$_X$ emissions and TROPOMI NO₂ exceeded 0.75. This suggests that the 108 spatial surrogates used by NEMO to spatially disaggregate NO$_X$ emissions from the U.S. county-level (5-200 km length scale) to the neighborhood level (~1 km length scale) are generally appropriate. However, this analysis also suggests some areas for improvement. Areas with dense warehouse operations appear to underestimate NO$_X$ emissions. Conversely, we find that NO$_X$ emissions in wealthy communities often appear to be overestimated using standard surrogates to disaggregate the inventory. Globally, we find spatial agreement between the EDGAR NO$_X$ inventory and NO₂ observed by TROPOMI, which indicates that most NO$_X$ sources are properly included in the inventory. The inventory and satellite measurements agreed most closely in the U.S ($\tau = 0.58$), moderately in East India ($\tau = 0.50$) and North China ($\tau = 0.52$), and least in South Africa ($\tau = 0.42$) and the Persian Gulf ($\tau = 0.45$). In the Persian Gulf region, future work should go into better understanding point source and marine NO$_X$ emissions, and in South Africa, TROPOMI suggests that some large sources are entirely missing from the inventory. This work provides a basis for the direct use of satellite data for NO$_X$ emissions inventory evaluation following appropriate filtering of the satellite data, without requiring a chemical transport model or complex statistical manipulation to translate between the satellite-derived tropospheric NO₂ columns and NO$_X$ emissions.

Highlights

- We apply a novel method to compare inventory-based emissions directly to TROPOMI satellite NO_2 data.
- In urban areas, there is excellent spatial correlation between satellite-measured NO_2 and the spatial surrogates used to downscale the NOx inventory.
- There are further opportunities to improve the NOx emissions inventory such as near environmental justice communities, warehousing operations, and intermodal facilities.

Graphical Abstract
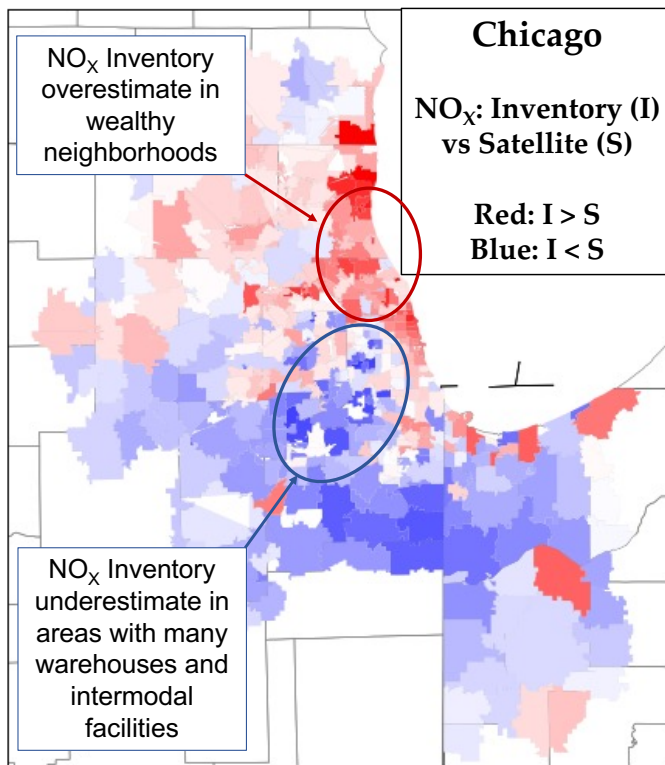
Introduction

Nitrogen dioxide (NO_2) is an air pollutant that adversely affects the human respiratory system (Health Effects Institute, 2022; Khreis et al., 2017) and leads to premature mortality (Burnett et al., 2004; He et al., 2020). NO_2 is also an important precursor for ozone and fine particulates, which also have serious health impacts. In urban areas, the majority of ambient NO_2 originates from NO_X emissions (=NO+NO2; most NO_X is emitted as NO which rapidly cycles to NO_2) during high-temperature fossil fuel combustion (Crippa et al., 2021). In many circumstances, end-of-pipe controls such as automotive catalytic converters (Koltsakis & Stamatelos, 1997) and selective catalytic reduction (Busca et al., 1998) can reduce the amount of NO_X emitted from engines and boilers by 70-99% but these technologies do not recover 100% of the NO_X generation during combustion. Because of this, NO_2 accumulates in cities and most urban areas have NO_2 concentrations that exceed the World Health Organization guideline of 5.3 ppb for an annual average (Anenberg et al., 2022).

To cost-effectively control NO_2, it is important to precisely know where NO_2 originates in cities. Mapping NO_X emissions typically requires the selection of emissions rates or factors for each source and distribution of the sources using spatial surrogates; both steps introduce considerable uncertainty into the estimates. While the types of activities that emit NO_X are known well (e.g., vehicles, fossil-fuel-fired power plants, etc.), not all vehicles or power plants have identical NO_X emissions and the magnitude of NO_X emissions from any source can vary dramatically by geographic region (Crippa et al., 2018; Janssens-Maenhout et al., 2015; McDuffie et al., 2020). Typically, NO_X emissions for an area are estimated by summing up the amount of fuel burned in that area and using sector-specific emissions factors or rates (McDuffie et al., 2020); for example, there are different emissions for vehicles versus industrial boilers, given the same mass of fuel burned. In some countries, such as India (Guttikunda et al., 2019; Saw et al., 2021), accurate data on fossil fuel consumption and sector emission rates are difficult to acquire. In other countries, fossil fuel consumption and sector emission rates can be accurate for national (~1000 km) or regional (~100 km) spatial scales, but additional information is needed to estimate NO_X emissions rates at neighborhood (~1 km) scales. Spatial surrogates are used to distribute county-level totals into sub-county levels, such as 12km or 4km grids (Eyth et al., 2006). An example of a spatial surrogate would be the location of a highway; NO_X emissions for roadways are typically allocated based on average miles traveled by a vehicle and the total number and type of vehicles on that type of road. For a regional or sub-regional scale, this assumption is often satisfactory, but much more detailed information is needed when trying to downscale a county-level inventory to individual roadways. Therefore, some of the assumptions used to spatially allocate NO_X emissions on a relatively coarse grid (~12 km) break down when trying to estimate NO_X emissions at the neighborhood spatial scale (~1 km). An independent way to map NO_X emissions – to discern when the original assumptions used to develop urban area NO_X emissions are valid – would be helpful to better understand the uncertainty in the originally calculated NO_X emissions. Remote sensing of air pollutants in urban areas can sometimes fill this role (Beirle et al., 2011, 2019; Finch et al., 2022; Goldberg, Lu, Oda, et al., 2019; Goldberg, Lu, Streets, et al., 2019; Liu et al., 2017; Pope et al., 2022; Xue et al., 2022).

NO$_2$ can be observed by remote sensing instruments due to its unique spectroscopic features within the 400 – 465 nm wavelength region (Vandaele et al., 1998). The Tropospheric Monitoring Instrument (TROPOMI) (Veefkind et al., 2012), launched in October 2017 aboard the Sentinel 5 Precursor satellite, has been measuring column amounts of NO$_2$ pollution at 5.5×3.5 km^2 spatial resolution (van Geffen, 2016). Because of this higher spatial resolution over predecessor instruments, such as GOME-2 (40×40 km^2 at nadir) (Richter et al., 2011), and OMI (24×13 km^2 at nadir) (Levelt et al., 2018), TROPOMI has ~50 daily satellite pixel measurements within a typical city (~1000 km^2) during clear skies; prior instruments only have 1-3 daily measurements within the borders of each city. This increased measurement capacity within a city allows us to discern spatial variability undetectable by previous instruments. Further, the data from the satellite instruments can be downscaled using a process called oversampling (de Foy et al., 2009; Sun et al., 2018), which re-grids the irregular satellite pixels to a standard and higher spatial resolution. The spatial resolution is thus effectively increased at the expense of the temporal resolution.

We seek to understand whether oversampled satellite data can directly inform estimated spatial heterogeneities of NO$_X$ emissions on a neighborhood scale, without relying on a chemical transport model (Canty et al., 2015; East et al., 2022; M. Li et al., 2021) or complex statistical inversion technique (Beirle et al., 2011, 2019, 2021; Goldberg, Lu, Streets, et al., 2019; Liu et al., 2022; Verstraeten et al., 2018). We oversample the satellite data over multiple years and filter to use data on stagnant wind days only – when the vertical overhead column should best capture the local emission influence – and then use this satellite average to evaluate the spatial representativeness of the 1×1 km^2 inventory-based Neighborhood Emission Mapping Operation (NEMO). This work is driven by recent advancements of both satellite instruments (oversampled pixels at $0.01° \times 0.01°$ resolution with improved signal-to-noise) and inventories (1-km spatial resolution inventories across the U.S and $0.1° \times 0.1°$ globally). The ability to directly compare satellite data to inventories without the need for complex modeling would enable air quality planners to evaluate and improve the NOx inventories they use to support air pollution policy decisions.

The first part of this analysis focuses on ten urban areas in the continental United States and then we expand the analysis to test cases in other global regions. For the urban-scale intercomparisons, we compare the satellite data averaged over May 2018 – Dec 2021 only during stagnant wind days to the NEMO NO$_X$ emissions dataset (Ma and Tong, 2022). For national scale intercomparisons, we compare the satellite annual average to the EDGAR annual NO$_X$ emissions inventory. As a bridge, we compare NEMO for selected cities to EDGAR, and NEMO to the satellite annual average, in order to determine the additional utility of both having a high spatial resolution inventory and filtering the satellite data based on wind speed.

2 Methods

2.1 TROPOMI

TROPOMI was launched by the European Space Agency (ESA) for the European Union's Copernicus S5P satellite mission on 13 October 2017. Data from the instrument became available on April 30, 2018, after an approximately 6-month calibration period. The satellite follows a sun-synchronous, low-earth (825 km) orbit with an equator overpass time of approximately 13:30 local solar time. TROPOMI measures total column amounts of several trace gases in the Ultraviolet-Visible-Near Infrared (UV-VIS-NIR) (e.g., NO_2 and HCHO) and Shortwave Infrared (SWIR) (e.g., CO) spectral regions (Veefkind et al., 2012). At nadir, pixel sizes are 3.5×7 km^2 (modified to 3.5×5.5 km^2 on August 6, 2019) with the edges having slightly larger pixels sizes (~14 km wide) across a 2600 km swath, equating to 450 rows (van Geffen et al., 2020). The instrument observes the swath approximately once every second and orbits the Earth in about 100 minutes, resulting in daily global coverage.

NO_2 slant column densities are derived from radiance measurements in the $405 - 465$ nm spectral window of the UV-VIS-NIR spectrometer (van Geffen et al., 2021). Satellite instruments observe NO_2 by comparing observed spectra with a reference spectrum to derive the amount of NO_2 in the atmosphere between the instrument and the surface; this technique is called differential optical absorption spectroscopy (DOAS) (Platt, 1994). Tropospheric vertical column density data, which represent the vertically integrated number of NO_2 molecules per unit area between the surface and the tropopause, are then calculated by subtracting the stratospheric portion and then converting the tropospheric slant column to a vertical column using an air mass factor (AMF) (Boersma et al., 2011). The AMF is a unitless quantity used to convert the slant column into a vertical column and is a function of the satellite viewing angles, solar angles, the effective cloud radiance fraction and pressure, the vertical profile shape of NO_2 provided by a chemical transport model simulation (for operational data the TM5-MP model is used at $1 \times 1°$ resolution) (Williams et al., 2017), and the surface reflectivity (for operational data, climatological Lambertian Equivalent Reflectivity is used at a $0.5 \times 0.5°$ resolution) (Kleipool et al., 2008). The operational AMF calculation does not explicitly account for aerosol absorption effects, which are accounted for in the effective cloud radiance fraction.

For our analysis we use the v2.3.1 Products Algorithm Laboratory (PAL) algorithm that was released in December 2021 (van Geffen et al., 2021) and includes updates to the cloud retrieval scheme (decrease in cloud pressure), the surface albedo (to avoid negative cloud fractions), and the quality flags (better screening of snow). The net result of the change in tropospheric vertical column NO_2 from v1.3 to v2.3.1 has been reported to be a +13% increase for cloud-free scenes that varies spatially and is higher in polluted areas (van Geffen et al., 2021).

For the domain-wide comparisons, we screened TROPOMI pixels for quality assurance flag values greater than 0.75 for the period between May 2018 – December 2021. For comparison with the annual NO_X emissions inventory, we gridded TROPOMI data to a $0.01° \times 0.01°$ resolution, to create a custom "Level-3" data product. This "Level 3" satellite product was then "aggregated up" to the zip code level ($1 - 50$ km spatial scales depending on region) for comparison with the NO_X emissions inventory.

2.2 ERA5 Re-analysis

We use the ERA5 re-analysis (Hersbach et al., 2020) of 100-m wind speed and direction between 16 – 21 UTC, which approximates the overpass time of TROPOMI over the continental United States. After averaging the wind estimates from these six hours together, we match the TROPOMI NO_2 satellite data to the ERA5 wind data, and filter to only use satellite data when the 100-m wind speed is less than 2 m per second. The ERA5 re-analysis data products are reported at a $0.25° \times 0.25°$ spatial resolution and the wind speed is interpolated, using bilinear interpolation, to the $0.01° \times 0.01°$ oversampled TROPOMI NO_2 grid.

2.3 NEMO Inventory-Based NOx Emissions

In this project, we the Neighborhood Emission Mapping Operation (NEMO), which is a 1-km anthropogenic emission dataset in the United States (Ma & Tong, 2022). This inventory uses the spatial surrogates recommended by the U.S. EPA (Eyth et al., 2006) – 108 spatial surrogates in total – to downscale the emissions from the county-level to a 1-km grid. Emissions are the 2017 annual total, which is the most current U.S. EPA National Emissions Inventory (NEI) that is available, and more representative of the 2018 – 2021 timeframe than the 2020 NEI which is planned to be the next NEI iteration. Any projection of NO_X emissions from 2017 to a future year, would rely on some type of assumption and would add additional uncertainty, and is therefore not appropriate for this analysis. For comparison with the gridded satellite data, the NEMO inventory-based NO_X emissions was "aggregated up" to the zip code level (~1 – 100 km^2 spatial scales depending on region) so that both are at the same spatial scale. Within urban areas, NEMO's high-resolution aspect is largely preserved since many zip codes are <10 km^2.

2.4 EDGAR NOx Inventory-Based Emissions

For our global analysis we use the Emissions Database for Global Atmospheric Research (EDGAR) version 6.1 inventory for NO_X which has a most current year of 2018 (Joint Research Centre, 2022). These are reported as annual NO_X emissions at $0.1° \times 0.1°$ spatial resolution from all anthropogenic activities, excluding large scale biomass burning. For the energy related sectors, the activity data are primarily based on statistics from the International Energy Agency. Globally, anthropogenic NO_X emissions have been relatively constant since 2012 (McDuffie et al., 2020) and in urban areas, they are dropping at a slow rate of 0 – 4 % per year (Goldberg et al., 2021). Therefore, use of a 2018 inventory in lieu of a 2019 inventory – which is currently not available – is appropriate for this analysis. For more information on how the EDGAR inventory is compiled, see (Crippa et al., 2018) with updates for version 6.1 noted here: https://edgar.jrc.ec.europa.eu/index.php/dataset_ap61. Supplementary Figure 1 compares the EDGAR inventory to the NEMO inventory in the New York City metropolitan area.

2.5 Urban Area Boundaries

For our ten U.S. focus cities, we define cities using metropolitan statistical areas (MSAs) established by the Office of Management and Budget and used by the U.S. Census Bureau (https://www.whitehouse.gov/wp-

). The ten focus cities were selected based on a combination of MSA population size (all are within the top 20 in the U.S) and geographic diversity (e.g., Denver selected over Philadelphia). All zip codes that are located within counties belonging to a particular MSA are used in our analysis. MSAs encompass not only the densely populated urban centers but also outlying suburban areas. For example, the Washington DC MSA includes not only the District of Columbia but also counties in Virginia, Maryland, and West Virginia. When comparing TROPOMI NO_2 to NEMO NO_X emissions for the U.S. portion of our study, we transform these datasets from their native ~1 km^2 resolution to zip code averages by averaging all grid cell centroids contained within a given zip code. If zip codes are too small to contain coincident grid cells, we inverse distance weight using the surrounding grid cells following Kerr et al. (2021).

2.6 Comparison between TROPOMI NO_2 and the Gridded Emissions Inventories

To compare TROPOMI and NEMO, three additional processing steps are needed to allow a direct comparison. The first step involves filtering satellite data to only include days with low wind speeds. We select satellite data only on days in which the 100-m wind speeds are less than 2 m per second (and effectively cloud-free using a quality assurance value of 0.75 or greater). During the May 2018 – Dec 2021 period, 5 – 50 % of the days per urban area (min: 5% in Chicago, max: 50% in Phoenix) (Supplementary Figure 2) have satellite measurements collocated in time with slow wind speeds, down from approximately 40 – 90% of the days if this wind speed filter was not applied. We apply this filter because NO_2 plume outflow from upwind sources on windy days (> 2 m/s) can create offsets between surface NO_X emissions and observed NO_2 column abundances by the satellite. In most cases, we do not expect this additional filtering to bias the results. One timeframe and area that this may have a biasing affect is during the spring and summer near large water bodies; lake/sea/ocean breezes tend to be stronger on warm days with weaker synoptic winds, so filtering for low wind speeds might have a biasing effect that is difficult to control for. To minimize this, we include data from all seasons. The second step of additional processing is to "aggregate up" both the satellite NO_2 and NO_X inventory-based datasets to the zip code level to account for population, to account for NO_X plume conversion to NO_2, and to account for better TROPOMI sensitivity in urban areas at very fine spatial scales (Goldberg et al., 2022). Although zip codes have varying populations, generally, aggregating to zip code will roughly normalize for population. Zip codes have smaller spatial scales within the center of cities and larger spatial scales in the suburban and peri-urban areas. Further, zip codes are easier to interpret by policymakers – a target audience of this analysis. Lastly, since NO_X emissions can have significant spatial variation within cities, we convert the NO_2 and NO_X datasets into units of "percentile within the urban area" for a more representative intercomparison.

The coarser spatial resolution of EDGAR (0.1° × 0.1°) and lack of zip code information on a global scale does not allow for a similar comparison as TROPOMI versus NEMO. For comparisons between TROPOMI and EDGAR, we compare the annual averages directly. For the TROPOMI versus EDGAR comparison, we do not filter out TROPOMI data with high wind speeds since filtering by wind speed globally is computationally expensive (but is being considered for future work) and aggregate to 0.5° × 0.5°. Since neither dataset is normally distributed, a linear correlation is not expected. To account for this, we use a Kendall rank correlation (τ) to test for agreement between

the two datasets – which similar to a Pearson correlation (r) varies between 0 and 1, with 0 being no agreement and 1 being perfect agreement.

3 Results

3.1 Continental US Intercomparison: EDGAR vs. TROPOMI

We first compare the global-scale 2018 EDGAR NO_X inventory ($0.1° \times 0.1°$) – the most recent year available – to the TROPOMI NO_2 2019 annual average for the continental United States gridded at the same spatial resolution (Figure 1). For a nationwide comparison, the spatial resolution of EDGAR ($0.1° \times 0.1°$) is more appropriate than the spatial resolution of NEMO (1 km) since NO_2 column abundances are often near the satellite detection limit in rural areas and the satellite is unable to capture the fine-scale spatial heterogeneities of NO_2 and NO_X emissions in rural areas. While inventory-based NO_X and satellite NO_2 are different quantities: an emission rate at the surface versus the amount of NO_2 mass in an atmospheric column, we expect there to be some correlation because the majority of NO_2 in the urban troposphere exists near the surface and the NO_2 lifetime is short (2 – 7 hr) during the early afternoon. Using this coarse spatial resolution, we find a good Kendall rank correlation ($\tau = 0.58$) between the two datasets. This suggests that the emissions inventory at a spatial resolution of $0.1° \times 0.1°$ is spatially disaggregated very well in the continental United States. This intercomparison also suggests that TROPOMI captures the relative magnitude of most large sources of NO_2, including emissions from medium-sized cities, highways, and shipping lanes. The performance at this spatial resolution is similar to the predecessor instrument, the Ozone Monitoring Instrument (Supplementary Figure 3). However, TROPOMI measurements have sharper NO_2 gradients than OMI when transecting polluted areas.
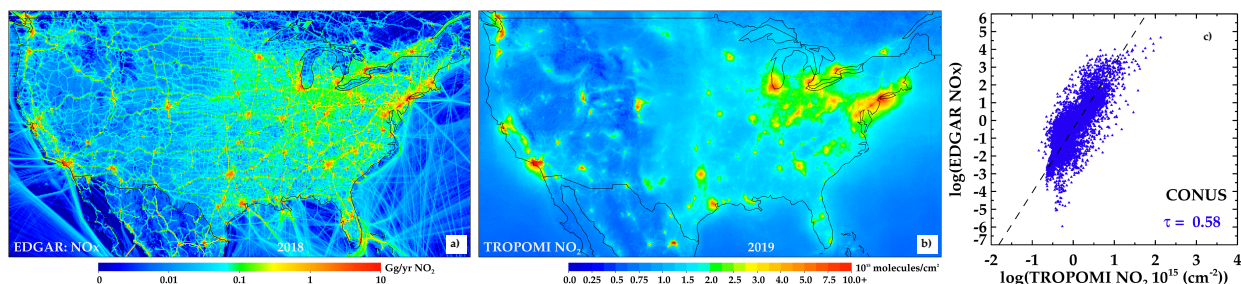
Figure 1. (a) The EDGAR NO_X emissions inventory for 2018 (Gg/yr NO_2) compared to (b) the annual average of TROPOMI NO_2 during 2019. (c) Scatterplot between the two datasets on a log-log scale.

3.2 Urban US Intercomparison: NEMO vs. TROPOMI

We then conduct a similar comparison at the urban scale ($0.01° \times 0.01°$) for ten US cities. In Figure 2, we show the inventory-based NO_X versus satellite NO_2 intercomparison for all ten cities. For brevity, here in the main text we only discuss the results from five of the cities (Figure 2): Chicago, New York City, Washington DC, Atlanta, and Los Angeles. The results for Phoenix, Houston, Dallas, Denver, and San Francisco are shown in Supplementary Figure 4. In the left hand panels, annual inventory-based NO_X emissions rates are shown and in the center panels the satellite column NO_2 from TROPOMI during stagnant wind days between May 2018 and Dec 2021 are shown. The scatterplots in the right hand column compare the relative zip code percentiles within the MSA between the satellite NO_2 (x-axis) and inventory-based NO_X emissions (y-axis). For 4 of the 5 cities (excluding Los Angeles), the r^2-value exceeds 0.75, which indicates that there is excellent agreement between the NEMO NO_X emissions inventory and TROPOMI NO_2.

This correlation is even better than the national intercomparison (Figure 1). Despite the excellent correlation, there are some neighborhoods within each urban area with disagreements, as shown by the red and blue dots, which correspond to potential inventory overestimates and underestimates respectively.
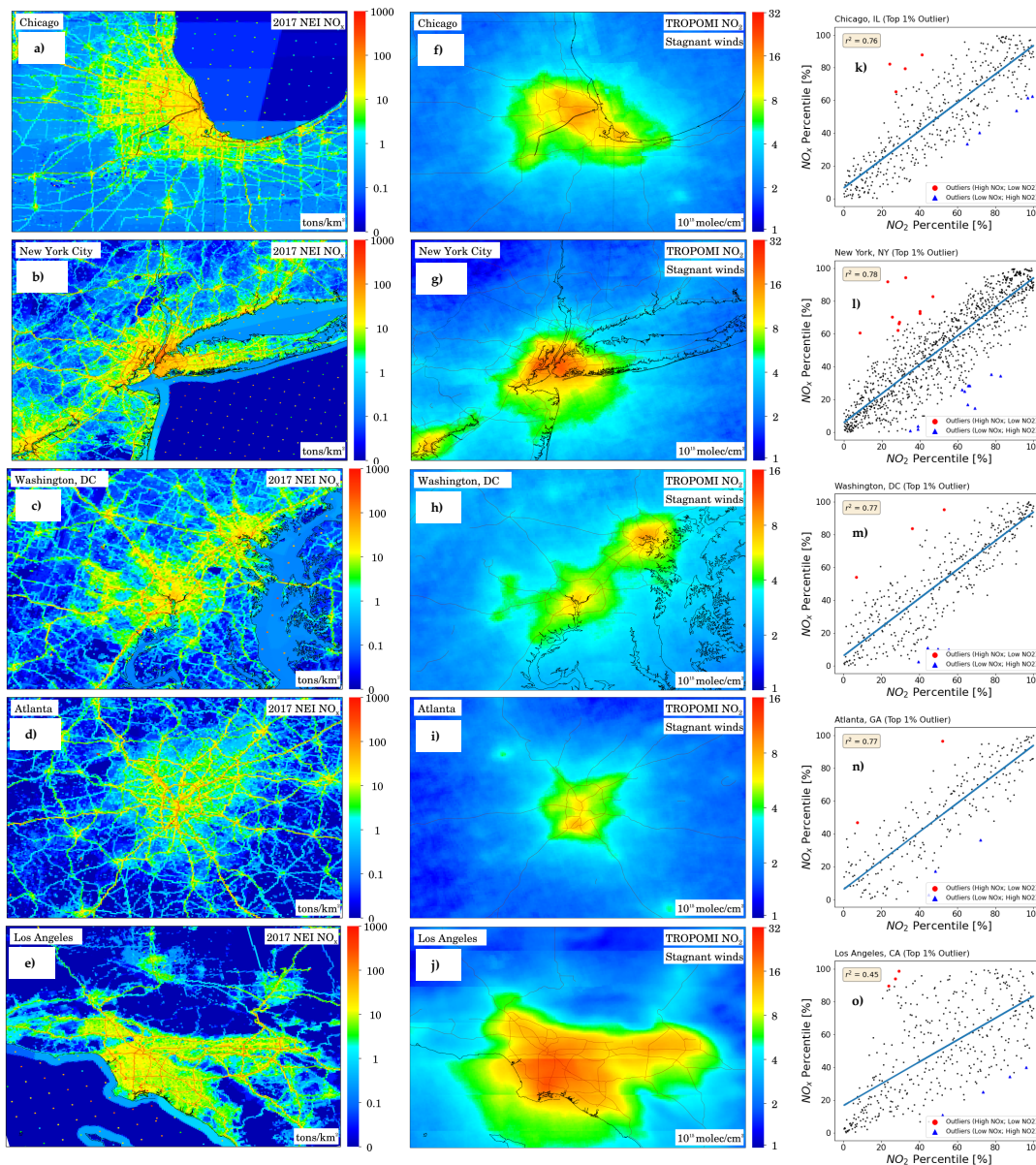
Figure 2. (a-e) The NEMO NO$_X$ emissions inventory for 2017 (Gg/yr NO$_2$) compared to (f-j) the 2018 – 2021 average of TROPOMI NO$_2$ during stagnant wind conditions (< 2 m/s at 100-m) and (k-o) Scatterplots between the two datasets when aggregated to the zip code within the MSA and plotted as percentiles. The five cities shown are: (Row 1) Chicago, (Row 2) New York City, (Row 3) Washington DC, (Row 4) Atlanta, (Row 5) Los Angeles. Scatterplots only show correlations within the MSA, which is a subset of the spatial domains shown in the spatial panels. Similar images for Phoenix, Houston, Dallas, Denver, and San Francisco can be found in Supp. Figure 4. The red dots in the scatterplots represent zip codes within the MSA in which the NO$_X$ percentile is substantially larger than the NO$_2$ percentile suggesting either a NO$_X$ inventory overestimate at the zip code or that TROPOMI is unable to fully quantify the NO$_2$ at that location. Conversely, the blue dots in the scatterplots represent zip codes within the MSA in which the NO$_X$ percentile is substantially smaller than the NO$_2$ percentile suggesting either a missing source in the NO$_X$ inventory or an influence of an upwind NO$_2$ plume at that location.

We now investigate the areas of potential inventory overestimates and underestimates. In Figure 3, we show the relative difference percentiles between inventory NO_X and satellite NO_2 amongst all zip codes for Chicago, New York City, and Atlanta, and then the same plot with only the largest differences highlighted. For Chicago, we find some notable differences in the inventory-based NO_X versus satellite NO_2 intercomparison. First, we observe that some of the point sources in the 2017 inventory are no longer operating in the 2018 – 2021 timeframe. This led to the largest discrepancies (inventory NO_X > satellite NO_2) in two the zip codes: 53158 (the location of the former Pleasant Prairie Power Plant, which retired in 2018) and 60088 (the location of the Waukegan Generating Station which has been phasing out and closed in June 2022). Next, we observe discrepancies, potential NO_X inventory overestimates, in wealthy neighborhoods. The zip code with the darkest red within the MSA, hinting at a NO_X inventory overestimate, is 60043 which is the wealthiest zip code in the MSA (and majority white). We find a particularly strong NO_X overestimate in two nearby zip codes within Chicago (60640 and 60660) that include a highway, Lakeshore Drive, that prohibits large diesel vehicles (and is surrounded by a community that is majority white). The spatial surrogates used to downscale emissions from the county-level to the zip code level may not be fully accurate with respect to the exact types of vehicles on the roadway nor do they account for socioeconomic status. We suggest that these are two necessary factors to accurately downscale NO_X emissions from the county-level in urban areas. We hypothesize that in the northern area of Chicago, wealthier residents are more likely to own newer vehicles with better catalytic converters, have more home efficiency measures, own electrified machinery/vehicles, and be more persistent in advocating against large emitters in their neighborhood. Therefore, the NO_X emissions in these neighborhoods may be lower in actuality than estimated in the gridded inventory-based NO_X emissions. Conversely, the zip codes with the most-blue within the MSA (60526, 60490, and 60446), hinting at a NO_X inventory-based underestimate, are west and southwestern of the city. These areas are more culturally diverse, and middle class. This area is also home to large industrial activities, including a quarry, and intermodal facilities, such as train depots and warehouses. The spatial surrogates used to downscale emissions from the county-level to a finer spatial scale may not fully account for idling vehicles and off-road equipment, such as forklifts and other heavy machinery operating at these facilities.

For New York City and Atlanta, we see similar themes emerge, albeit less pronounced, perhaps because these cities are less segregated. In the New York City MSA, there are red shades in Manhattan which suggests a NO_X inventory overestimate, while blue shades in Staten Island suggest a NO_X inventory underestimate implying a small spatial misallocation of NO_X emissions within the city. We theorize that the spatial downscaling might not fully account for a heavier reliance on public transportation by those living in Manhattan relative to Staten Island residents. There is also a potential NO_X emissions overestimate in the wealthier suburbs of Bergen, Westchester, and Suffolk Counties noted by the preponderous of red shades in these counties. There are similar findings in the Atlanta MSA; there is also a potential NO_X emissions overestimate in the wealthier suburbs of northern Fulton and Forsyth Counties. Zip codes with dense warehouses, such as in central New Jersey and south of the Atlanta-Hartsfield airport, appear to have a NOx inventory underestimate. In some instances, especially in New York City, we see some disagreements along uninhabited coastline which is most likely related to NO_2 plume outflow, but could also be related to a spatial misallocation of boat/ship emissions.
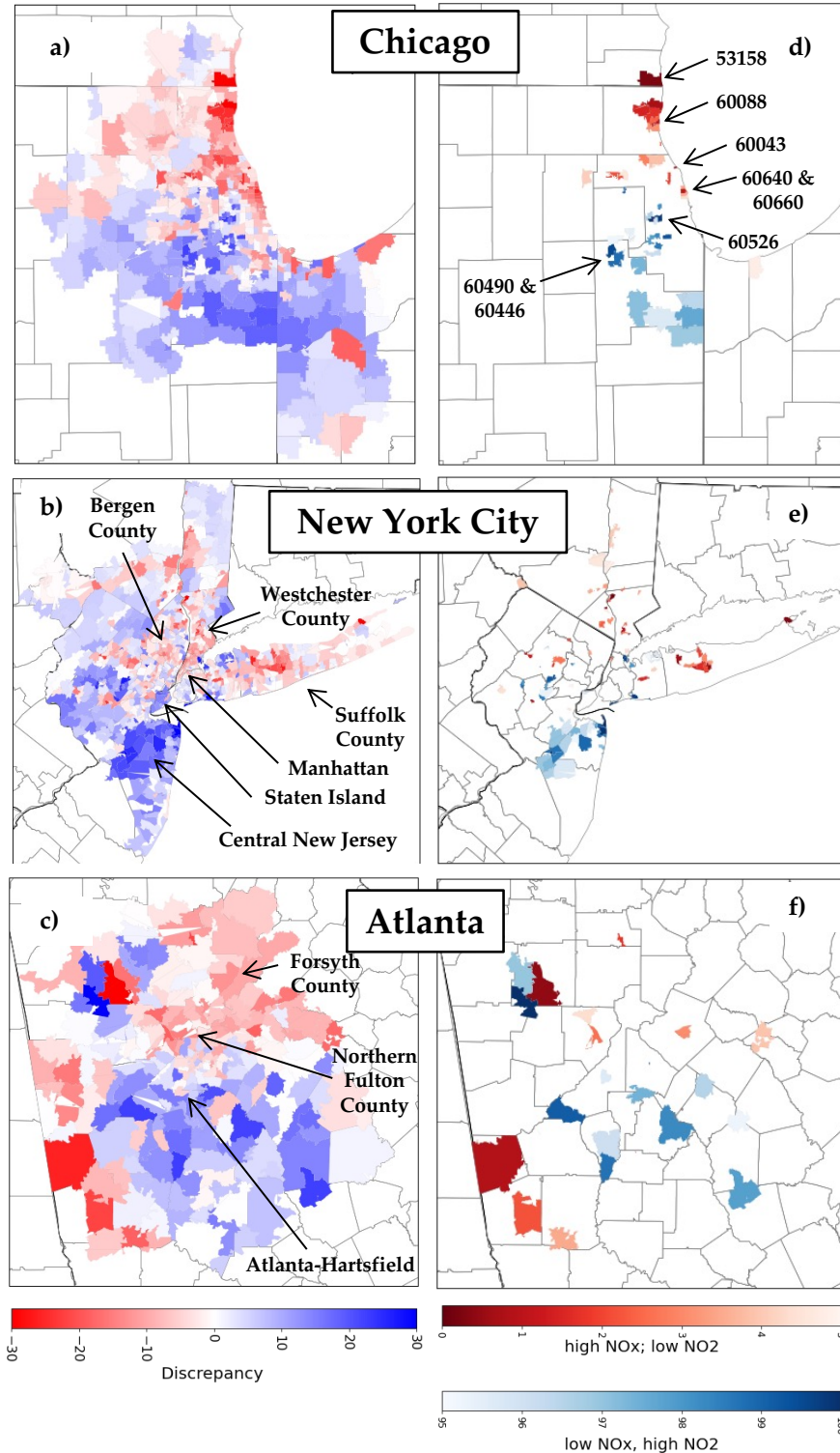
Figure 3. (a-c) Inventory NO$_X$ versus satellite NO$_2$ discrepancy, or distance from one-to-one line of the scatterplot of the zip codes from Figure 2. (d-f) Using the values from the left panels, only the top 5% outliers in each direction within the MSA are shown. Red discrepancies indicate areas where the NOx inventory is disproportionately larger than the satellite NO$_2$. Blue discrepancies indicate areas where the satellite NO$_2$is disproportionately larger than the NOx inventory. The three cities shown are: (Row 1) Chicago, (Row 2) New York City, (Row 3) Atlanta. Similar images for Phoenix, Houston, Dallas, Denver, Washington DC, San Francisco, and Los Angeles can be found in Supp. Figure 5.

Los Angeles is an outlier in this intercomparison project. We find that the NO_X versus NO_2 intercomparison yields an $r^2 = 0.45$, which is substantially lower than any other US city, including San Francisco, which has somewhat similar climatology, or Denver, which has similar topography. We attribute the poor correlation to the complex terrain that traps the pollution locally for days/weeks. It is possible that the Los Angeles intercomparison would benefit from a high-resolution meteorological model, instead of the ERA5 $0.25° \times 0.25°$ re-analysis. However, we hypothesize that the persistent stagnation and accumulation of NO_2 over time within the South Coast basin may make the methodology outlined herein unfeasible. We suggest that this method should not be applied to any city that is in a "bowl-shaped" valley, such as Los Angeles, where pollution consistently accumulates for multiple days. Therefore, we do not attempt to make any conclusion from the inventory-based NO_X versus satellite NO_2 intercomparison for Los Angeles.

When we instead use the 2019 annual average of satellite NO_2 observations without restricting to days with stagnant wind only, there are unexpected findings. In some cities, most notably Chicago and New York City, the correlation between satellite NO_2 and inventory NO_X increases: in Chicago it increases from $r^2 = 0.76$ to $r^2 = 0.84$ and in New York City it increases from $r^2 = 0.77$ to $r^2 = 0.82$ (Supplementary Figure 6). This finding is counterintuitive because this analysis includes days with stronger winds that would disperse the NO_2 away from sources quickly. One possibility for the increase in r^2 is that the 2019 annual average has approximately twice as many satellite observations as the 2018-2021 average when filtered for low wind speeds, and therefore has less random noise leading to stronger correlation. It is also possible that a 2019 average is more representative of the 2017 average than average over the 2018 – 2021 timeframe. However, a different explanation appears more likely. On days with stagnant winds, the largest NO_2 is 10 – 50 km WSW of both Chicago (near intermodal facilities, warehouses, and industrial operations) and New York City (Newark port / warehouses). However, the prevailing wind direction when averaged over the full year, is also WSW (Supplementary Figure 7) so this effectively moves the NO_2 from the NOx emissions on the SW side to directly over the city, giving the appearance that the largest NOx is originating over the city center when in fact the largest NOx emissions are SW of the city. Since population density is a large driver of the inventory downscaling – from the county-level to 1-km – it is possible that the prevailing wind direction is falsely giving an appearance of better agreement between the inventory and satellite data. The Atlanta area provides a test of this hypothesis because that city does not have a strong prevailing wind direction and a moderate wind (Supplementary Figure 7), and for Atlanta the r^2-value decreases from $r^2 = 0.78$ to $r^2 = 0.74$, which is what we expected when using an annual average not filtered for wind speed. Therefore, filtering for wind speed likely does give a more realistic intercomparison between the satellite data and the inventory.

3.3 Global Intercomparison: EDGAR vs. TROPOMI

Our analysis for the United States suggests that the NO_X emissions reported at the national and regional scales are overall appropriately spatially disaggregated to neighborhood scales. Considering that we do not fully account for the influences of meteorology in our method, having r^2-values exceeding 0.73 in many urban areas is promising. We now shift to evaluating how this analysis performs in other global areas.

In Figure 4, we show four regions: Persian Gulf, South Africa, east India, and central China; the global comparison is shown in Supplementary Figure 8. These four regions were chosen due to their known large anthropogenic NO_X sources and previous research suggesting potential discrepancies in the inventories (Barkley et al., 2017; Goldberg et al., 2021; Guttikunda et al., 2019; Hakkarainen et al., 2021; Meng Li et al., 2018; Miyazaki et al., 2017). Regions with large amounts of intentional biomass burning, such as Latin America, central Africa, and north India were excluded from this analysis since the EDGAR inventory does not group these intentional burning practices as anthropogenic sources. For each region, we generate scatterplots between the EDGAR inventory and the 2019 TROPOMI NO_2 annual average (with no wind filtering) and plot on a log-log scale. Of the four regions that were evaluated, we find worst agreement between the EDGAR inventory and TROPOMI NO_2 in South Africa ($\tau = 0.42$) followed by the Persian Gulf ($\tau = 0.45$) region. In East India and North China, we find moderate agreement ($\tau = 0.50$ and $\tau = 0.52$ respectively) suggesting that the spatial disaggregation of the NO_X inventory is better in India and China than in South Africa and the Persian Gulf, but worse than in the United States. Areas in the Persian Gulf and South Africa have the most opportunities for NO_X inventory improvement and will be discussed more in the following paragraphs.
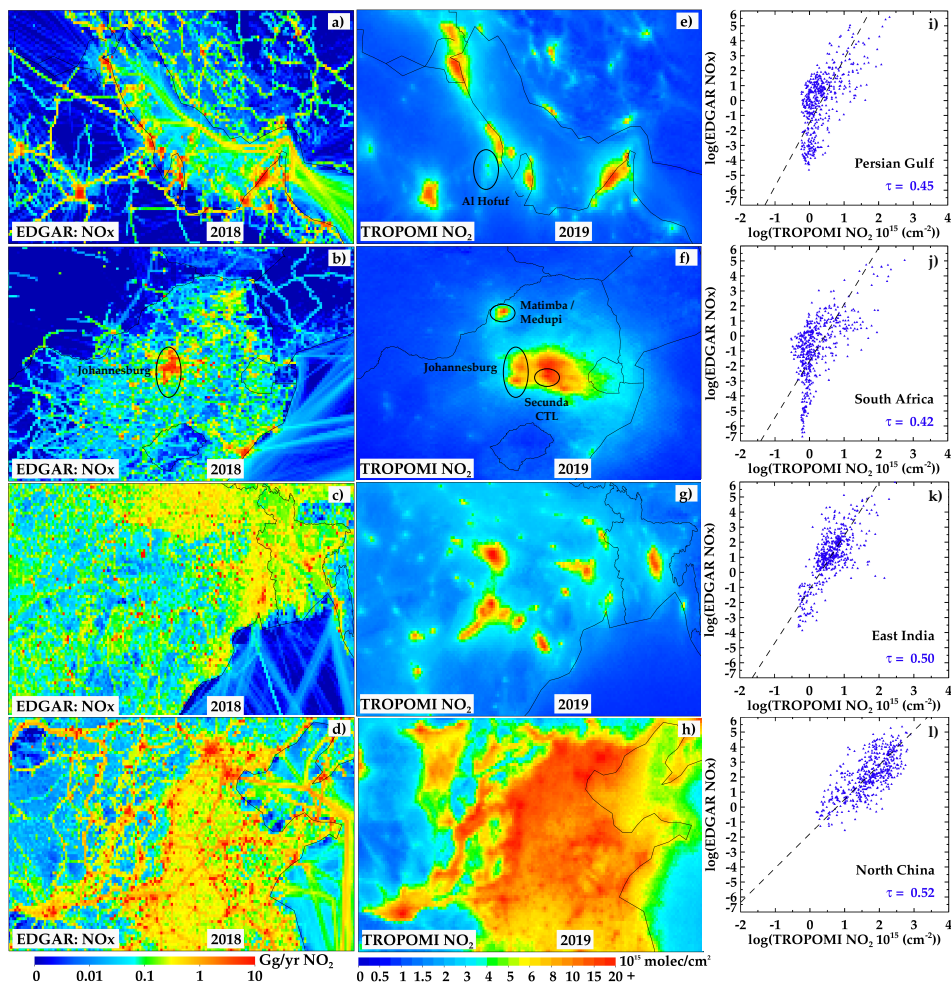
Figure 4. (a-d) The EGDAR NO_X emissions inventory for 2018 (Gg/yr NO_2) compared to (e-h) the annual average of TROPOMI NO_2 during 2019. (i-l) Scatterplot between the two datasets on a log-log scale. Four regions are shown: (Row 1) Persian Gulf, (Row 2) South Africa, (Row 3) East India, and (Row 4) North China.

In the Persian Gulf region, we find the biggest disagreements directly over the Gulf itself. There are no known biases in the satellite NO_2 algorithm in polluted areas over open water relative to over land that would contribute to these signals (Thompson et al., 2019). While it is known that many ships traverse this area, these ships may be traveling in a different location than the assumed ship track. This would lead to a more dispersed NO_2 plume, and poor agreement between the satellite and inventory from a spatial standpoint. Additionally, some of the locations of the inventory point sources have some spatial mismatching with the satellite NO_2 data. For example, 200km west of Qatar in Saudi Arabia near Al Hofuf, there are four natural gas plants (Qurayyah, Faras, Shedgum, and Uthmaniyah), but only a weak satellite NO_2 signal in this location suggesting that these plants may operate less than estimated in the inventory or are more efficient than estimated.

In South Africa, comparison of inventory-based NO_X with the satellite NO_2 finds large disagreements that raise concerns with the EDGAR inventory in this area. NO_X emissions from the Secunda CTL syngas operation – the largest single CO_2 emitter in the world – is missing from the EDGAR inventory. Also, the NO_X emissions from the Matimba / Medupi power station complex appears to be underestimated by EDGAR, which is consistent with (Reuter et al., 2019). Conversely, in nearby Botswana it appears that EDGAR is suggesting large NO_X sources that do not exist or emit NO_X at much lower rates. The locations and NO_X emissions of other sources in South Africa appear to be roughly correct – high density of coal power plants E of Johannesburg – but that the NO_X emissions – due to operational time or efficiency – may be incorrect. It is feasible that the total NO_X emissions on a country-level may be approximately correct but that the spatial allocation to each individual plant may be off.

Discussion

This analysis demonstrates that TROPOMI NO_2 when oversampled during stagnant wind days over multiple years can be an effective surrogate to estimate the spatial heterogeneities of NO_X emissions within an urban area. In nine of the ten US cities analyzed here, r^2-values between the NEMO NO_X inventory and TROPOMI NO_2 apportioned by percentile exceeded 0.75. This finding suggests that the 108 spatial surrogates used to spatially disaggregate NO_X emissions from the U.S. county-level (~25 km length scale) to the neighborhood level (~1 km length scale) are generally appropriate, especially for modeling applications with a 12 km spatial resolution or coarser. However, this analysis also suggests some areas for improvement in the inventories. We find that areas that have a large density of warehouse operations appear to have an underestimate of NO_X emissions. This may be partially due to the proliferation of large warehouse construction since 2017, the year for which the NEI was developed. Nonetheless, this analysis suggests that characterizing the sources and magnitudes of NO_X emissions near warehouses should be a priority for future research, as consumers and retailers continue to push for same-day home delivery of goods. Conversely, we find some evidence that NO_X emissions in wealthy communities may be overestimated using standard surrogates to disaggregate the inventory. We theorize that wealthier residents are more likely to own newer vehicles with better catalytic converters, own electrified tools/vehicles, and have more resources in advocating against large emitters, such as diesel truck routes and industrial operations, in their neighborhood.

In many gridded emissions inventories, population-related data are used as surrogates to downscale emissions. While this approach is appropriate in some cases when other information, such as ownership of fossil-fuel-based machinery is not known, our results suggest that including some aspect of socioeconomic status may further improve the spatial allocation of the emissions. This is an important finding for two reasons. First, this suggests that the standard assumptions to downscale NO_X emissions may not be fully appropriate for some applications, such as evaluating pollution disparities between advantaged and disadvantaged communities. Second, this finding suggests that more work needs to be done to develop emission reduction strategies that target lower socioeconomic neighborhoods rather than applying citywide standards that may disproportionately benefit neighborhoods that already have relatively low emissions.

Globally, we find that there is reasonably good spatial agreement between the EDGAR NO_X inventory and NO_2 observed by TROPOMI when aggregated to $0.5° \times 0.5°$ resolution, which indicates that the majority of NO_X sources are properly included in the inventory. The inventory and satellite measurements agreed most closely in the U.S, moderately in India and China, and least in the Persian Gulf and South Africa regions. In the Persian Gulf region, future work should advance understanding point source and marine NO_X emissions. In South Africa, we find that some large sources were entirely missing from the inventory.

From a scientific perspective, this work demonstrates that satellite data can be useful in evaluating a NO_X emissions inventory without the use of a chemical transport model or complex statistical manipulation under certain conditions. For example, such comparisons should use annual average satellite data because there would be too much missing data, random noise, and unaccounted meteorological effects if only one day or one month were used. If possible, we find that it's more appropriate to isolate days with slow wind speeds and average them together, rather than averaging all days without accounting for winds. This is because winds disperse NOx, leading to spatial offsets between where the NOx was emitted and where the satellite will observe it. In addition, the climatological/prevailing wind direction, such as climatological southwesterly winds in New York City and Chicago, can give the appearance of a false agreement.

This work demonstrates how satellite data can be helpful for policymakers in characterizing the spatial distribution of NO_X emissions without a chemical transport model. The improved spatial resolution and reduced noise of TROPOMI enables a new way to evaluate NOx emission inventories in urban areas at scales previously not possible. Future instruments, such as TEMPO and Sentinel 4, with similar pixel sizes, but more numerous observations (hourly measurements instead of a single daily measurement), may allow this comparison to be done on shorter timeframes.

Acknowledgments

References

Anenberg, S. C., Mohegh, A., Goldberg, D. L., Kerr, G. H., Brauer, M., Burkart, K., et al. (2022). Long-term trends in urban NO2 concentrations and associated paediatric asthma incidence: estimates from global datasets. *The Lancet Planetary Health*, *6*(1), e49–e58. https://doi.org/10.1016/S2542-5196(21)00255-2

Barkley, P. M., González Abad, G., Kurosu, P. T., Spurr, R., Torbatian, S., & Lerot, C. (2017). OMI air-quality monitoring over the Middle East. *Atmospheric Chemistry and Physics*, *17*(7). https://doi.org/10.5194/acp-17-4687-2017

Beirle, S., Boersma, K. F., Platt, U., Lawrence, M. G., & Wagner, T. (2011). Megacity Emissions and Lifetimes of Nitrogen Oxides Probed from Space. *Science*, *333*(6050), 1737–1739. https://doi.org/10.1126/science.1207824

Beirle, S., Borger, C., Dörner, S., Li, A., Hu, Z., Liu, F., et al. (2019). Pinpointing nitrogen oxide emissions from space. *Science Advances*, *5*(11), eaax9800. https://doi.org/10.1126/sciadv.aax9800

Beirle, S., Borger, C., Dörner, S., Eskes, H. J., Kumar, V., de Laat, A., & Wagner, T. (2021). Catalog of NOx emissions from point sources as derived from the divergence of the NO2 flux for TROPOMI. *Earth Syst. Sci. Data*, *13*, 2995–3012. https://doi.org/10.5194/essd-13-2995-2021

Boersma, K. F., Eskes, H. J., Dirksen, R. J., Van Der A, R. J., Veefkind, J. P., Stammes, P., et al. (2011). An improved tropospheric NO2 column retrieval algorithm for the Ozone Monitoring Instrument. *Atmospheric Measurement Techniques*, *4*(9), 1905–1928. https://doi.org/10.5194/amt-4-1905-2011

Burnett, R. T., Stieb, D., Brook, J. R., Cakmak, S., Dales, R., Raizenne, M., et al. (2004). Associations between short-term changes in nitrogen dioxide and mortality in Canadian cities. *Archives of Environmental Health*, *59*(5), 228–236. https://doi.org/10.3200/AEOH.59.5.228-236

Busca, G., Lietti, L., Ramis, G., & Berti, F. (1998). Chemical and mechanistic aspects of the selective catalytic reduction of NO(x) by ammonia over oxide catalysts: A review. *Applied Catalysis B: Environmental*, *18*(1–2), 1–36. https://doi.org/10.1016/S0926-3373(98)00040-X

Canty, T. P., Hembeck, L., Vinciguerra, T. P., Anderson, D. C., Goldberg, D. L., Carpenter, S. F., et al. (2015). Ozone and NOx chemistry in the eastern US: Evaluation of CMAQ/CB05 with satellite (OMI) data. *Atmospheric Chemistry and Physics*, *15*(19), 10965–10982. https://doi.org/10.5194/acp-15-10965-2015

Crippa, M., Guizzardi, D., Muntean, M., Schaaf, E., Dentener, F., van Aardenne, J. A., et al. (2018). Gridded emissions of air pollutants for the period 1970--2012 within EDGAR v4.3.2. *Earth System Science Data*, *10*(4), 1987–2013. https://doi.org/10.5194/essd-10-1987-2018

Crippa, M., Guizzardi, D., Pisoni, E., Solazzo, E., Guion, A., Muntean, M., et al. (2021). Global anthropogenic emissions in urban areas: patterns, trends, and challenges. *Environmental Research Letters*, *16*(7), 074033. https://doi.org/10.1088/1748-9326/AC00E2

East, J. D., Henderson, B. H., Napelenok, S. L., Koplitz, S. N., Sarwar, G., Gilliam, R., et al. (2022). Inferring and evaluating satellite-based constraints on NOx emissions estimates in air quality simulations. *Atmos. Chem. Phys*, *22*, 15981–16001. https://doi.org/10.5194/acp-22-15981-2022

Eyth, A., Ran, L., Partheepan, R., & Yarwood, G. (2006). New tools to generate spatial surrogate and speciation profile inputs to SMOKE.

Finch, D. P., Palmer, P. I., & Zhang, T. (2022). Automated detection of atmospheric NO2 plumes from satellite data: A tool to help infer anthropogenic combustion emissions. *Atmospheric Measurement Techniques*, *15*(3), 721–733. https://doi.org/10.5194/AMT-15-721-2022

de Foy, B., Krotkov, N. A., Bei, N., Herndon, S. C., Huey, L. G., Martínez, A.-P., et al. (2009). Hit from both sides: tracking industrial and volcanic plumes in Mexico City with surface measurements and OMI SO2 retrievals during the MILAGRO field campaign. *Atmospheric Chemistry and Physics*, *9*(24), 9599–9617. https://doi.org/10.5194/acp-9-9599-2009

van Geffen, J. (2016). TROPOMI ATBD of the total and tropospheric NO2 data products, (2). Retrieved from https://sentinel.esa.int/documents/247904/2476257/Sentinel-5P-TROPOMI-ATBD-NO2-data-products

van Geffen, J., Boersma, K. F., Eskes, H. J., Sneep, M., ter Linden, M., Zara, M., & Veefkind, J. P. (2020). S5P TROPOMI NO2 slant column retrieval: method, stability, uncertainties and comparisons with OMI. *Atmospheric Measurement Techniques*, *13*(3), 1315–1335. https://doi.org/10.5194/amt-13-1315-2020

van Geffen, J., Eskes, H. J., Compernolle, S., Pinardi, G., Verhoelst, T., Lambert, J.-C., et al. (2021). Sentinel-5P TROPOMI NO2 retrieval: impact of version v2.2 improvements and comparisons with OMI and ground-based data. *Atmospheric Measurement Techniques*, *15*(7), 2037–2060. https://doi.org/10.5194/AMT-15-2037-2022

Goldberg, D. L., Lu, Z., Streets, D. G., de Foy, B., Griffin, D., McLinden, C. A., et al. (2019). Enhanced Capabilities of TROPOMI NO2: Estimating NOx from North American Cities and Power Plants. *Environmental Science & Technology*, *53*(21), 12594–12601. https://doi.org/10.1021/acs.est.9b04488

Goldberg, D. L., Lu, Z., Oda, T., Lamsal, L. N., Liu, F., Griffin, D., et al. (2019). Exploiting OMI NO2 satellite observations to infer fossil-fuel CO2 emissions from U.S. megacities. *Science of The Total Environment*, *695*, 133805. https://doi.org/10.1016/j.scitotenv.2019.133805

Goldberg, D. L., Anenberg, S. C., Lu, Z., Streets, D. G., Lamsal, L. N., E McDuffie, E., & Smith, S. J. (2021). Urban NOx emissions around the world declined faster than anticipated between 2005 and 2019. *Environmental Research Letters*, *16*(11), 115004. https://doi.org/10.1088/1748-9326/ac2c34

Goldberg, D. L., Harkey, M., de Foy, B., Judd, L., Johnson, J., Yarwood, G., & Holloway, T. (2022). Evaluating NOx emissions and their effect on O3 production in Texas using TROPOMI NO2 and HCHO. *Atmospheric Chemistry and Physics*, *22*(16), 10875–10900. https://doi.org/10.5194/acp-22-10875-2022

Guttikunda, S. K., Nishadh, K. A., & Jawahar, P. (2019). Air pollution knowledge assessments (APnA) for 20 Indian cities. *Urban Climate*, *27*, 124–141. https://doi.org/10.1016/j.uclim.2018.11.005

Hakkarainen, J., Szelag, M. E., Ialongo, I., Retscher, C., Oda, T., Crisp, D., et al. (2021). Analyzing nitrogen oxides to carbon dioxide emission ratios from space: A case study of Matimba Power Station in South Africa. *Atmospheric Environment: X, 10*, 100110. https://doi.org/10.1016/j.aeaoa.2021.100110

He, M. Z., Kinney, P. L., Li, T., Chen, C., Sun, Q., Ban, J., et al. (2020). Short- and intermediate-term exposure to NO2 and mortality: A multi-county analysis in China. *Environmental Pollution*, *261*, 114165. https://doi.org/10.1016/j.envpol.2020.114165

Health Effects Institute. (2022). *Systematic Review and Meta-analysis of Selected Health Effects of Long-Term Exposure to Traffic-Related Air Poll*. Retrieved from https://www.healtheffects.org/system/files/hei-special-report-23-executive-summary_0.pdf

Hersbach, H., Bell, B., Berrisford, P., Hirahara, S., Horányi, A., Muñoz-Sabater, J., et al. (2020). The ERA5 global reanalysis. *Quarterly Journal of the Royal Meteorological Society*, *146*(730), 1999–2049. https://doi.org/10.1002/qj.3803

Janssens-Maenhout, G., Crippa, M., Guizzardi, D., Dentener, F., Muntean, M., Pouliot, G., et al. (2015). HTAP_v2.2: a mosaic of regional and global emission grid maps for 2008 and 2010 to study hemispheric transport of air pollution. *Atmospheric Chemistry and Physics*, *15*(19), 11411–11432. https://doi.org/10.5194/acp-15-11411-2015

Joint Research Centre. (2022). Emissions Database for Global Atmospheric Research version 6.1. Retrieved from https://edgar.jrc.ec.europa.eu/index.php/dataset_ap61

Khreis, H., Kelly, C., Tate, J., Parslow, R., Lucas, K., & Nieuwenhuijsen, M. (2017). Exposure to traffic-related air pollution and risk of development of childhood asthma: A systematic review and meta-analysis. *Environment International*, *100*, 1–31. https://doi.org/10.1016/j.envint.2016.11.012

Kleipool, Q. L., Dobber, M. R., de Haan, J. F., & Levelt, P. F. (2008). Earth surface reflectance climatology from 3 years of OMI data. *Journal of Geophysical Research Atmospheres*, *113*(18), 1–22. https://doi.org/10.1029/2008JD010290

Koltsakis, G., & Stamatelos, A. (1997). Catalytic automotive exhaust aftertreatment. *Progress in Energy and Combustion Science*, *23*(1), 1–39. https://doi.org/10.1016/s0360-1285(97)00003-8

Levelt, P. F., Joiner, J., Tamminen, J., Veefkind, J. P., Bhartia, P. K., Zweers, D. C. S., et al. (2018). The Ozone Monitoring Instrument: Overview of 14 years in space. *Atmospheric Chemistry and Physics*, *18*(8), 5699–5745. https://doi.org/10.5194/acp-18-5699-2018

Li, M., McDonald, B. C., McKeen, S. A., Eskes, H. J., Levelt, P., Francoeur, C., et al. (2021). Assessment of Updated Fuel-Based Emissions Inventories Over the Contiguous United States Using TROPOMI NO 2 Retrievals. *Journal of Geophysical Research: Atmospheres*, *126*(24), e2021JD035484. https://doi.org/10.1029/2021JD035484

Li, Meng, Klimont, Z., Zhang, Q., Martin, R. v., Zheng, B., Heyes, C., et al. (2018). Comparison and evaluation of anthropogenic emissions of SO2 and NOx over China. *Atmospheric Chemistry and Physics*, *18*(5), 3433–3456. https://doi.org/10.5194/acp-18-3433-2018

Liu, F., Beirle, S., Zhang, Q., Van Der A, R. J., Zheng, B., Tong, D., & He, K. (2017). NOx emission trends over Chinese cities estimated from OMI observations during 2005 to 2015. *Atmospheric Chemistry and Physics*, *17*(15), 9261–9275. https://doi.org/10.5194/acp-17-9261-2017

Liu, F., Tao, Z., Beirle, S., Joiner, J., Yoshida, Y., Smith, S. J., et al. (2022). A new method for inferring city emissions and lifetimes of nitrogen oxides from high-resolution nitrogen dioxide observations: a model study. *Atmos. Chem. Phys*, *22*, 1333–1349. https://doi.org/10.5194/acp-22-1333-2022

Ma, S., & Tong, D. Q. (2022). Neighborhood Emission Mapping Operation (NEMO): A 1-km anthropogenic emission dataset in the United States. *Scientific Data 2022 9:1*, *9*(1), 1–10. https://doi.org/10.1038/s41597-022-01790-9

McDuffie, E. E., Smith, S. J., O'Rourke, P., Tibrewal, K., Venkataraman, C., Marais, E. A., et al. (2020). A global anthropogenic emission inventory of atmospheric pollutants from sector- and fuel-specific sources (1970–2017): an application of the Community Emissions Data System (CEDS). *Earth System Science Data*, *12*(4), 3413–3442. https://doi.org/10.5194/essd-12-3413-2020

Miyazaki, K., Eskes, H. J., Sudo, K., Folkert Boersma, K., Bowman, K. W., & Kanaya, Y. (2017). Decadal changes in global surface NOxemissions from multi-constituent satellite data assimilation. *Atmospheric Chemistry and Physics*, *17*(2), 807–837. https://doi.org/10.5194/acp-17-807-2017

Platt, U. (1994). Differential Optical Absorption Spectroscopy (DOAS). In *Air monitoring by spectroscopic techniques* (p. 531). Wiley-IEEE.

Pope, R. J., Kelly, R., Marais, E. A., Graham, A. M., Wilson, C., Harrison, J. J., et al. (2022). Exploiting satellite measurements to explore uncertainties in UK bottom-up NOx emission estimates. *Atmospheric Chemistry and Physics*, *22*(7), 4323–4338. https://doi.org/10.5194/ACP-22-4323-2022

Reuter, M., Buchwitz, M., Schneising, O., Krautwurst, S., O'dell, C. W., Richter, A., et al. (2019). Towards monitoring localized CO_2 emissions from space: co-located regional CO_2 and NO_2 enhancements observed by the OCO-2 and S5P satellites. *Atmospheric Chemistry and Physics*, *19*, 9371–9383. https://doi.org/10.5194/acp-19-9371-2019

Richter, A., Begoin, M., Hilboll, A., & Burrows, J. P. (2011). An improved NO_2 retrieval for the GOME-2 satellite instrument. *Atmospheric Measurement Techniques*, *4*(6), 1147–1159. https://doi.org/10.5194/amt-4-1147-2011

Saw, G. K., Dey, S., Kaushal, H., & Lal, K. (2021). Tracking NO_2 emission from thermal power plants in North India using TROPOMI data. *Atmospheric Environment*, *259*, 118514. https://doi.org/10.1016/j.atmosenv.2021.118514

Sun, K., Zhu, L., Cady-Pereira, K. E., Chan Miller, C., Chance, K. V., Clarisse, L., et al. (2018). A physics-based approach to oversample multi-satellite, multi-species observations to a common grid. *Atmospheric Measurement Techniques Discussions*, *11*(12), 1–30. https://doi.org/10.5194/amt-2018-253

Thompson, A. M., Stauffer, R. M., Boyle, T. P., Kollonige, D. E., Miyazaki, K., Tzortziou, M. A., et al. (2019). Comparison of Near-Surface NO_2 Pollution With Pandora Total Column NO_2 During the Korea-United States Ocean Color (KORUS OC) Campaign. *Journal of Geophysical Research: Atmospheres*, 2019JD030765. https://doi.org/10.1029/2019JD030765

Vandaele, A. C., Hermans, C., Simon, P. C., Carleer, M., Colin, R., Fally, S., et al. (1998). Measurements of the NO_2 absorption cross-section from 42 000 cm−1 to 10 000 cm−1 (238–1000 nm) at 220 K and 294 K. *Journal of Quantitative Spectroscopy and Radiative Transfer*, *59*(3–5), 171–184. https://doi.org/10.1016/S0022-4073(97)00168-4

Veefkind, J. P., Aben, I., McMullan, K., Förster, H., de Vries, J., Otter, G., et al. (2012). TROPOMI on the ESA Sentinel-5 Precursor: A GMES mission for global observations of the atmospheric composition for climate, air quality and ozone layer applications. *Remote Sensing of Environment*, *120*(2012), 70–83. https://doi.org/10.1016/j.rse.2011.09.027

Verstraeten, W. W., Boersma, K. F., Douros, J., Williams, J. E., Eskes, H., Liu, F., et al. (2018). Top-Down NOX Emissions of European Cities Based on the Downwind Plume of Modelled and Space-Borne Tropospheric NO_2 Columns. *Sensors*, *18*(9), 2893. https://doi.org/10.3390/s18092893

Williams, J. E., Folkert Boersma, K., Le Sager, P., & Verstraeten, W. W. (2017). The high-resolution version of TM5-MP for optimized satellite retrievals: Description and validation. *Geoscientific Model Development*, *10*(2), 721–750. https://doi.org/10.5194/gmd-10-721-2017

Xue, R., Wang, S., Zhang, S., He, S., Liu, J., Tanvir, A., & Zhou, B. (2022). Estimating city NOx emissions from TROPOMI high spatial resolution observations – A case study on Yangtze River Delta, China. *Urban Climate*, *43*, 101150. https://doi.org/10.1016/J.UCLIM.2022.101150